Liu, E., Dore, John C., Webber, J. Beau W., Khushalani, S., Findenegg, G.H. and Hansen, Thomas (2006) *Neutron diffraction and NMR relaxation studies of structural variation and phase transformations for water/ice in SBA-15 silica: I. The over-filled case.* Journal of Physics: Condensed Matter, 18 (44). pp. 10009-10028. ISSN 0953-8984.

Neutron diffraction and NMR relaxation studies of structural variation and phase transformations for water/ice in SBA-15 silica. I: The over-filled case

E Liu[1,5], J C Dore[1], J B W Webber[1,4], D Kushalani[1,6], S Jähnert[2], G H Findenegg[2], and T Hansen[3]

[1] School of Physical Sciences, University of Kent, Canterbury ,CT2 7NH, UK

[2] Department of Chemistry, Technical University Berlin, Strasse des 17. Juni 124, D-10623 Berlin, Germany.

[3] Institut Laue Langevin, BP156, F38042 Grenoble Cedex, France.

[4] now at Institute of Petroleum Engineering, Heriot Watt, Edinburgh, EH14 4AS.

[5] now at School of Chemistry, University of Manchester, Oxford Road, Manchester, M13 9PL.

[6] now at the Tata Institute for Fundamental Research, Mumbai India.

E-mail: `J.C.Dore@kent.ac.uk`

Abstract. Neutron diffraction and NMR relaxation measurements have been made of water/ice in SBA-15, a mesoporous silica constituting an ordered array of cylindrical mesopores of pore diameter ~86 Å, over the temperature range 180K to 300K in a cooling and heating cycle. The over-filled sample shows the initial formation of hexagonal ice on the outside of the silica grains, followed by the nucleation of cubic ice inside the pores at a lower temperature. Neutron scattering profiles for the cubic ice peaks are significantly broadened and indicate a defective structure, as observed in previous experiments on ice formation in sol-gel and MCM-type silicas. Below the pore freezing temperature the intensity of the cubic ice peaks exhibit a significant increase, down to the lowest experimental temperature, indicating a reversible conversion of defective ice to ordered ice crystals. The peak profile analysis for the two ice patterns indicates a systematic variation in the position as a function of temperature, giving values of the expansion coefficients that are slightly lower than other measurements for the bulk phase. NMR results on proton relaxation as a function of temperature indicate the presence of a mobile phase for temperatures below pore freezing that supports the view that there is inter-conversion between brittle and plastic phases of ice.

1. Introduction

The properties and phase behaviour of water are substantially modified by confinement in the narrow pores of a hydrophilic mesoporous solid such as silica. Studies of the freezing of water in sol-gel silicas (Wright and Sommerdijk, 2000) have shown the depression of nucleation point and the subsequent formation of defective cubic ice in pores of less than 300 Å diameter. Neutron diffraction studies (Dore *et al.*, 1999) have revealed a freezing point depression of $\sim$ 45 K in the ordered cylindrical pores of MCM-41 and MCM-48 silicas (Beck *et al.*, 1992) with pore diameters in the region of 35Å. It is, consequently, of interest to investigate the behaviour of water and its nucleation to ice in equally well-defined silica materials with wider pores, such as SBA-15 (Zhao *et al.*, 1998a,b). This material has the same pore structure as MCM-41 but with pore diameters of typically 60 – 100 Å. The freezing/melting of water in a series of MCM-41 and SBA-15 materials of different pore widths has been studied by differential scanning calorimetry (DSC) (Schreiber *et al.*, 2001) and small-angle x-ray scattering, revealing significant differences in the freezing behaviour of water for over-filled and partially-filled pores of MCM-41 and SBA-15.

    In the present paper we report a neutron diffraction study of the behaviour of water and ice in a sample of SBA-15 silica with a pore diameter of $\sim$ 86 Å, over a wide temperature range; some complementary NMR relaxation measurements are also included. The data presented here form part of a comprehensive investigation of water/ice in SBA-15 silicas using neutron diffraction and NMR techniques. The present case is for an 'over-filled' sample and additional measurements for several 'partially-filled' states using the same sample material will be presented in subsequent papers.

2. Theory and Experiment

2.1. Neutron formalism

Neutron diffraction has been used extensively for the study of confined water under a range of conditions (Dore, 2000). The data for D_2O water may be used to evaluate the liquid structure factor $S_m(Q,T)$ and the composite pair correlation function g(r).

    In the case of water confined in silica, there is additional scattering from the silica that must be subtracted from the observations and the resultant function also includes a water-silica cross-term that may be significant for studies involving small pore sizes. In the present case this contribution is relatively small and it is still convenient to use a temperature difference approach and to evaluate the structural change relative to a chosen reference temperature, T_0, through the function:-

$$\Delta D_M(Q, \Delta T) = S_M(Q,T) - S_M(Q,T_o) \tag{1}$$

where, $\Delta T = T - T_o$.

    For the solid crystalline phase, the structure factor is more conventionally written as S(*hkl*) and gives Bragg peaks corresponding to the reflections defined by the Miller

indices h, k and l. Diffraction measurements involve the coherent interference of scattered waves so that equation 2.1 applies to the polycrystalline solid as well as the disordered liquid. Consequently, the difference function technique can be applied to circumstances where there is a phase change in the material. This approach is often useful in the detailed investigation of the structural changes occurring in the confined material as a function of temperature and eliminates some systematic uncertainties in the data treatment.

The peak profile also provides a useful indicator of the crystallite size through the Debye-Scherer relation, which may be written as :-

$$\sigma = \frac{4 \pi K_{DS}}{D} \qquad (2)$$

where σ is the peak width (as a function of Q), for a crystallite of dimension D; K_{DS} is a geometric constant that depends on crystal shape and is close to unity for a spherical distribution. The shapes of the crystallites in the present experiment are not well defined as they may be comparable to the pore size with a roughly spherical shape or they could extend along the cylinder axis and have a large aspect ratio. The diffraction broadening results from the restricted number of lattice planes contributing to the constructive interference for a specific scattering vector and is therefore dependent also on crystal orientation. In the present case, it is assumed that there is random orientation of the pore axes so that the observed intensity profile is an equally-weighted average over all directions. However, the pore matrix consists of a disordered hexagonal lattice of aligned cylinders so the situation is more complex if the independently-grown crystallites in neighbouring pores are correlated. This system has been treated in a recent paper by Morineau and Alba-Simionesco (Morineau and Alba-Simionesco, 2003) in order to evaluate the excluded volume term and possible effects from correlations between the crystallites and the silica matrix. They apply the formalism to the structural analysis of benzene in SBA-15 silicas with pores of 65 Å diameter and show that care must be exercised in deducing information about changes in the inter-molecular correlations of the confined phase relative to those of the bulk phase. These principles are also relevant to the current studies but the larger pore size of the silica and the fact that a differential approach is adopted for the analysis and interpretation of the nucleated phases means that the effects are much smaller and can be neglected to first-order. However, a detailed examination of the peak profiles and their change with temperature is of interest and will be the subject of future work; it is beyond the scope of this first publication.

2.2. Nuclear magnetic resonance techniques

There is a range of several different NMR techniques that can provide information on the structural features of porous systems. In particular, NMR is a sensitive technique for distinguishing between the solid and liquid phases of a liquid imbibed into the pores. One technique is to measure the change in the time constant of the transverse relaxation (T_2) signal of a liquid in the pores, although this method requires the value

of the relaxivity interaction between the liquid and the pore wall material to be known (Brownstein and Tarr, 1977; Strange *et al.*, 2003).

An alternative technique is NMR cryoporometry (Strange, Rahman and Smith, 1993; Webber, Strange and Dore, 2001) which is used to investigate the pore distribution function by determining the amount of liquid phase present as a function of temperature. The magnitude of the transverse relaxation signal (T_2), at a time when the signal from the solid has decayed, is used to indicate the quantity of liquid in the sample material.

The melting point of the pore liquid is depressed by ΔT, as given by the Gibbs-Thomson relation:-

$$\Delta T = {K_{GT}}/{X} \tag{3}$$

where K_{GT} is a constant that depends on the liquid, the pore geometry and the wetting nature of the pore walls. X is a dimension that defines the effective size of the pore (Webber, 2003). The technique is analogous to differential scanning calorimetry, DSC, but has a number of advantages that have been discussed in the earlier papers (Webber and Dore, 2004).

The value of the relaxation rate also gives information about the dynamics of the protons in the confined material as a function of temperature (Booth and Strange, 1998). The large difference in the T_2 values distinguishes between the liquid and solid phases in the cryoporometry studies but the actual relaxation rates themselves give additional information about the proton mobility. Other techniques, such as those based on the modification of the spin-echo signal by applied magnetic field gradients can be used to provide further information relating to self-diffusion in the pore network and may also help to distinguish between translational and rotational motion.

2.3. Preparation and characterisation of the SBA-15 sample

SBA-15 silica was synthesized by the method reported by Zhao et al. (Zhao *et al.*, 1998a,b) using a technical grade poly(ethylene-oxide)-poly(propylene-oxide)-poly(ethylene-oxide) triblock copolymer (Pluronic P103, BASF USA, Mount Olive, NJ) as the structure-directing agent. A solution of 8 g P103 and 13 ml of H_2SO_4 (97%) in 480 ml of Milli-Q water was prepared (pH <2), and 9.2 ml of tetraethyl orthosilicate (TEOS, ABCR, purity 97%) was added as the silicate precursor under vigorous stirring at 40 °C. The polymer-silica composite, which formed as a fine precipitate was aged at elevated temperature (90 °C) for 24 hrs, washed with pure water, dried in air and slowly heated to 550 °C to completely remove the organic component. Details of the thermal treatment and calcination of the sample are given elsewhere (Schreiber *et al.*, 2001).

The pore structure of the calcined SBA-15 silica was characterized by nitrogen adsorption using a Gemini 2375 volumetric gas adsorption analyzer (Micromeritics). Samples were dried and out-gassed at 120 °C for 45 min at a pressure below 0.1 mbar and reweighed before the measurement. The adsorption and desorption isotherms (77 K) are shown in Figure 1.
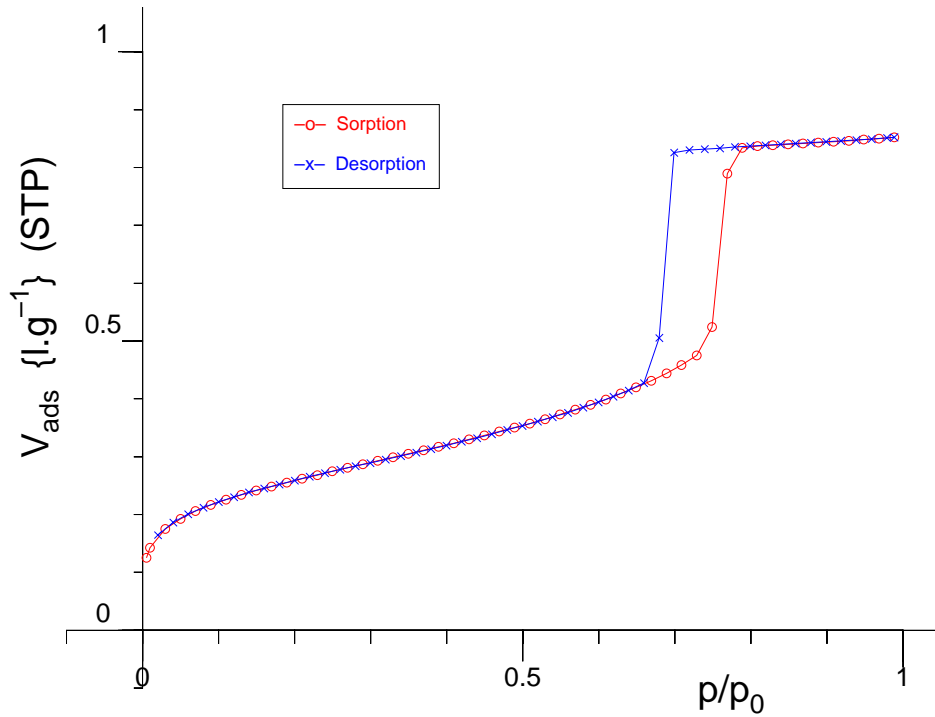
Figure 1. Nitrogen gas adsorption and desorption isotherms for the SBA-15 silica sample.

The specific surface area a_s was determined by the BET multi-point method in a range of relative pressures p/p_0 from 0.05 to 0.31, using $a_m(N_2) = 0.162$ nm^2. The specific pore volume v_p was derived from the plateau of the isotherm (at $p/p_0 = 0.98$), using the density of liquid nitrogen at 77 K (0.808 g cm^{-3}). The mean pore diameter D was derived from the pore condensation pressure $(p/p_0)_c = 0.758$ (adsorption branch) on the basis of the Kelvin equation and the FHH equation for the thickness of the adsorbed film. Resulting values of specific surface area a_s, pore volume v_p and mean pore width D are given in Table 1. A repeat measurement after 30 months gave the same pore radius but $\sim 6\%$ lower values of a_s and v_p than those given in Table 1.

The periodic pore structure of SBA-15 was also characterised by small-angle X-ray diffraction using synchrotron radiation (DESY, Hasylab, Hamburg, Germany; beamline A2). The Bragg peaks conform to a 2D hexagonal lattice (space group $P6mm$). The resulting value of the lattice constant a_0 is given in Table 1.

Combining the SAXD data with the BET data, the thickness of the pore walls along the pore centre connection line, $w = a_0 - D$, is estimated as 23 Å for the present sample.

Evidence from X-ray diffraction (Impéror-Clerc *et al.*, 2000; Zickler *et al.*, 2006), solid-state NMR (Shenderovich *et al.*, 2003) and nitrogen adsorption studies (Kruk *et al.*, 1997) indicates some microporosity of the pore walls of SBA-15, either as a microporous corona of the cylindrical pores (Impéror-Clerc *et al.*, 2000) or resulting from corrugations of the pore walls (Shenderovich *et al.*, 2003). It has been shown

Sample	N$_2$ sorption			SAXD
	a_s {m^{2}g^{-1}}	v_p {cm^{3}g^{-1}}	D {Å}	a_0 {Å}
SBA-15	900 ± 45	1.3 ± 0.06	86 ± 5	109.9

Table 1. Characterization of SBA-15 by nitrogen adsorption and SAXD. BET specific surface area a_s, specific pore volume v_p, pore diameter D, and lattice parameter a_0; the value of D is derived from the adsorption branch of the hysteresis loop and the t-layer equation $t/nm = 0.43 \, [(-5)/\ln(p/p_0)_c]^{1/3}$.

(Schreiber *et al.*, 2006) that the nitrogen adsorption isotherms and small-angle neutron scattering data for adsorbed nitrogen films in SBA-15 can be represented by simple geometric models of corrugated pore walls. For the present sample, the values of of a_s and v_p (Table 1) indicate that the nitrogen monolayer volume represents 24 % of the total pore volume, i.e., nearly one in four molecules is in direct contact with the pore wall at complete pore filling. However, for water the situation appears to be different from nitrogen. The water vapor adsorption isotherm in SBA-15 at room temperature does not exhibit a high-affinity region at low pressures, but a weak linear increase up to $p/p_0 \approx 0.5$. The pore volume as determined by water adsorption is about 10 % smaller than the value obtained by nitrogen adsorption. These findings seem to indicate that water molecules are not penetrating into the porous corona of the pore wall at room temperature.

NMR cryoporometry measurements were made of the pore volume, using water as the probe liquid. The sample was dried at 120 $^\circ$C overnight at ambient pressure, distilled water added, and the sample left to equilibrate for some days. Since the total volume of the liquid in the sample is known from weighings, the volume in the pores can be directly determined from the ratio of the amplitudes for the plateau in the NMR signal amplitudes for the melting event of the pore liquid to that for the melting event of the bulk liquid. Corrections were made for T$_2$ relaxation effects (Webber, 2000), giving v_p = 1.11 ml.g^{-1} for water in this sample of SBA-15. It seems likely that this measurement protocol is not accessing the pore volume associated with p/p$_0$ < 0.05 in figure 1. It should be noted that the volume determined from NMR cryoporometry measurements is all associated with an "open-loop" plot characteristic of the free liquid, compared with the value of $\sim$ 0.6 ml.g^{-1} (STP) in figure 1. This result therefore adds further support to the view that possible complications due to microporosity are negligible in the present case.

2.4. Experimental procedure for neutron studies

For the neutron experiments, D$_2$O water was added to the dry silica powder and was left to equilibrate for $\sim$3 hrs. This produced an 'over-filled' sample with a filling factor, f, larger than unity. The exact filling factor depends on the assumptions made about the available volume for the water in the pores, with the v_p values from nitrogen gas

adsorption, water vapour adsorption and NMR Cryoporometry giving slightly different values for f. However, a separate evaluation may be made directly from the relative neutron scattering intensities for the water signal before and after the nucleation of the water on the outside of the pores. The latter method gives higher values with a weighted mean of f=1.27 ±0.05. This difference may reflect the fact that the separate methods are probing the pore volume in a different manner or possibly that a full equilibration had not been achieved in the case of the neutron measurements. Nevertheless, it is clear that there is excess water on the outside of the pore grains that has properties that relate closely to bulk water. It is therefore appropriate to take a nominal value of 1.15 ±0.10 as the filling factor, to be consistent with all estimates. The exact value does not materially affect the interpretation of the results.

The sample was placed inside a 5mm diameter vanadium container. The cell was mounted on a centre stick of a standard helium cryostat and installed on the D20 diffractometer (Hansen, 2004) at the Institut Laue Langevin, Grenoble. The diffractometer uses a thermal beam from the reactor and a neutron wavelength of 2.400Å was chosen for this experiment. The scattered neutrons are detected in a 150° position-sensitive detector so that the whole of the diffraction pattern was measured over a Q-range of $0.3 - 5.1$ Å^{-1}. The high neutron flux on this instrument meant that a measurement of only two minutes was sufficient to give a diffraction pattern with good statistics as shown in Fig 2, for various water/ice phases.
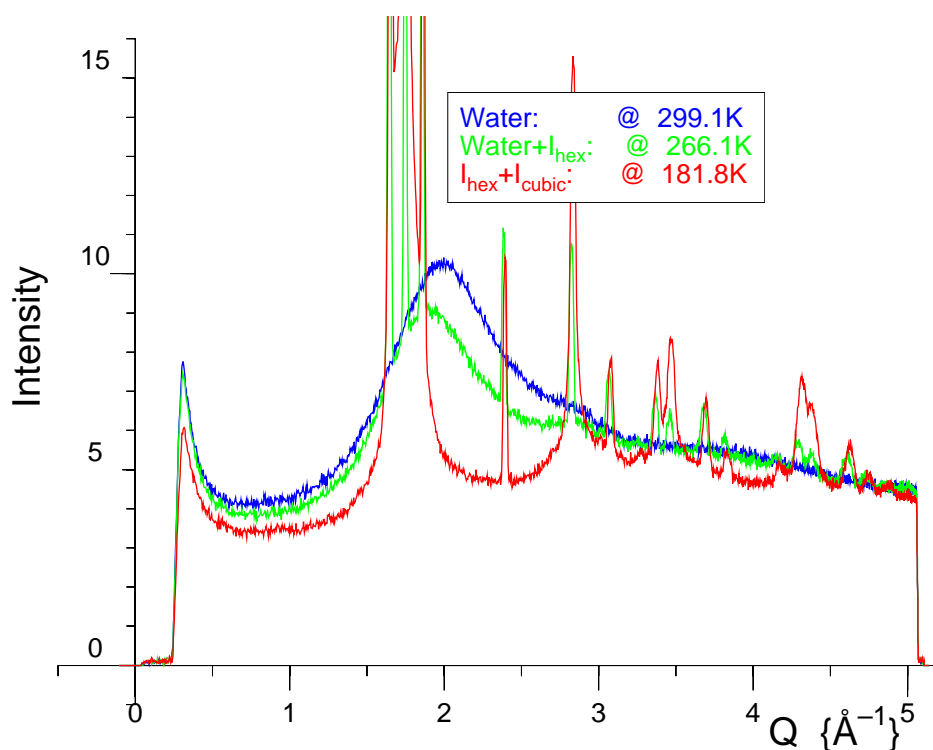
Figure 2. Diffraction patterns for the dry silica and the silica with water/ice, showing the three temperature regions corresponding to different phases.

The scattering from the silica was subtracted from that of the wet sample to give the diffraction pattern for the D_2O; there is a negligible contribution from the water-silica cross-term for the total intensity pattern. Furthermore, the temperature-derivative function, $\Delta D_M(Q, \Delta T)$, eliminates this term to first order.

Typical scans were taken with a temperature ramp of 0.6K/min in either cooling or heating mode. For the experiments on this particular sample starting at 300 K, an initial cooling run was made down to 180 K, followed by a heating run at the same ramp rate. The scattered intensity profile in the detector was output every two minutes, giving a total of 230 independent spectra. Standard methods were used to correct the datasets for detector efficiency and to produce a set of normalised diffraction patterns, calibrated against the recorded temperature.

The recorded temperature does not correspond exactly to the actual mean temperature in the irradiated volume due to the poor thermal conductivity of the sample material. The mass of sample required for neutron scattering ($\sim$ 0.25 g) is much greater than that required for DSC ($\sim$ 10 mg), and since the warming and cooling rates are comparable, a significantly broader transition is recorded for the phase transitions using neutron scattering compared with DSC. However, the temperature lag during the time sequence simply shifts the effective temperature relative to the recorded temperature. The high resolution of the Bragg peaks from the ice enabled the peak positions to be compared for both the cooling and the heating runs and displayed an apparent temperature difference of $\sim$3 K for the two runs. This value gives $\pm$1.5 K as the correction to the recorded temperature arising from the thermal lag. With this offset term, the effective relative temperature of the sample is defined to an accuracy of $\pm$0.1 K and an absolute accuracy of $\pm$0.5 K. A preliminary report of this work has been given by Liu (Liu, 2003).

2.5. Experimental procedure for NMR studies

Further information on the state of the confined water/ice can be obtained by measurement of the T_2 relaxation time for H_2O water as a function of temperature. Earlier papers give some of the details (Dore *et al.*, 2004; Webber and Dore, 2004) but the essential information relevant to the current NMR work is briefly presented.

The variation of the NMR T_2 relaxation rate with temperature was measured on the same apparatus as previously used for NMR cryoporometry studies (Webber *et al.*, 2001). Over the lower to middle temperature range the relaxation rate was measured by recording the Bloch decay from the water/ice. The data were fitted using the sum of a Gaussian function appropriate to the brittle ice and an exponential function appropriate to the more mobile component. The measured value was then corrected for the natural T_2^* due to the gradients in the B_0 magnetic field. At medium to higher temperatures, data were also recorded using a Carr-Purcell-Meiboom-Gill (CPMG) sequence that gives an echo chain. The results are discussed in Section 3.6.

For these NMR cryoporometry measurements warming rates of 0.2, 0.1 and 0.05

K.min^{-1}, and 2τ measurement times of 1, 2 and 4 ms were used for different runs, and this data was used to provide second-order corrections for the measured melting-point depression and pore volume respectively, using the techniques discussed earlier (Webber, 2000).

3. Data Analysis

There are several distinct regions for the temperature scans. On a cooling ramp, the first region [A] involves the liquid phase that extends from 300K down to 270.5K when nucleation of the supercooled D_2O to hexagonal ice occurs on the external surface of the silica grains. The second region [B] involves the coexistence of this hexagonal ice with an equilibrium liquid phase inside the pore volume extending down to 258K. The third region [C] commences when the confined water nucleates to a defective form of cubic ice, which occurs primarily over the temperature range 266K to 255K.

The diffraction pattern shows that this form of ice continues to grow for temperatures extending down to 185K. This sequence is reversed on the heating ramp although the transition temperatures are somewhat different. The cubic ice in the pores finally melts completely at 274K. The correction for temperature lag in the cooling and heating runs is given in Section 2.3 and gives a precision of ±0.2 K in the relative scale, the temperature offset due to the use of a temperature ramp (and a thermocouple spatially displaced from the sample) being closely defined by the final melting temperature of the hexagonal ice around the grains at 286K.

In order to analyse the diffraction pattern quantitatively, it is convenient to fit the peaks using a Gaussian profile represented by four parameters and defined by the expression:-

$$I(Q) \quad = \quad \frac{A}{\sigma\sqrt{\pi/2}} \exp\left[\frac{2(Q-Q_0)^2}{\sigma^2}\right] \quad - \quad I_B, \tag{4}$$

where A is the area of the peak with a width σ, centred at Q_0, and I_B is a constant representing the general background intensity. It was convenient to group together five separate recorded spectra to improve the statistical accuracy of each data-set prior to the use of a standard χ^2- fitting routine.

The analysis of the coupled datasets involves the determination of the parameter values as a function of temperature but a free search over five parameters is not needed for most of the sequence. The σ parameter defining the peak width is primarily dependent on the instrument resolution and the effects of broadening due to crystallite size. In the case of the hexagonal ice peaks it was therefore found that this value could be kept constant throughout the temperature range while the peak position Q_0 varied systematically with T. Subsequent analysis then showed that the values of the peak and background intensities, A and I_B, could also be set at constant values. This observation is indicative of the fact that the amount of ice on the outside of the silica granules did

not change significantly with temperature and the only effect was for a contraction of the crystal lattice as the temperature was reduced.

The behaviour of the ice peaks for the confined phase is more complex as the diffraction broadening effects are larger, the peaks are not all symmetric and there is a systematic change in the peak intensities with temperature. Furthermore, the temperature region where the cubic ice is formed also contains the peaks for the hexagonal ice, which are changing position with temperature. Some peaks correspond to hexagonal ice only and it was possible to confirm that the behaviour of these peaks conformed to the features observed in the upper temperature region. It was found that the analysis of compound peaks could therefore be conducted by using the parameter values obtained from the treatment of the hexagonal ice alone. This treatment showed that the combined peak (no 5) consisted of two peaks and could be fitted with Gaussian shapes of different width. The analysis procedure could therefore be carried out by fitting two overlapping Gaussian curves using the standard parameters from the hexagonal ice for one set and allowing variable parameters for the other set. The A, Q_0 and I_B values were found to vary with temperature for the second set of values due to the growth and displacement of this broader Gaussian peak but the variation was found to be systematic with T, enabling meaningful parameters to be extracted.

The triplet peak for the region 1.6-1.8 Å^{-1} poses another problem as the peak profiles appear markedly asymmetric and, although they have an isolated Gaussian form for the hexagonal ice phase, they are strongly overlapping for the cubic ice phase. The profile is itself of some interest but there is currently no established analytic form that can be used to decompose the data into individual components. A systematic study of this composite peak will be presented in a separate paper (Seyed-Yazdi *et al.*, in preparation).

The temperature difference treatment leads to a function that includes a differential term arising from the displacement of the hexagonal ice peaks with temperature. However, the parameter values for this contribution are known and it is consequently possible to correct the datasets for this effect. The results show that the cubic ice profile does not exhibit any significant shape changes but the intensity and the position of the central peak varies systematically with temperature. These interesting characteristics show that the growth of the cubic ice phase extends over a wide temperature range and can give important information about the phase transformation occurring for the water/ice in the pores. The results are discussed in more detail in the following section, where they divided into three different temperature ranges, A, B, C.

3.1. The liquid water phase.

The initial cooling phase [A] from 300K concerns the structural changes occurring in both the surface water on the grains and the confined water in the pores. The neutron data are conventionally analysed (Dore, 2000), subtracting the dry silica data from the measured intensity distribution. Figure 3a shows the variation of the pattern with

temperature, indicating the displacement of the main peak. The temperature difference function ΔD_M (Q, ΔT) (eqn. 3) is shown in figure 3b for these datasets.
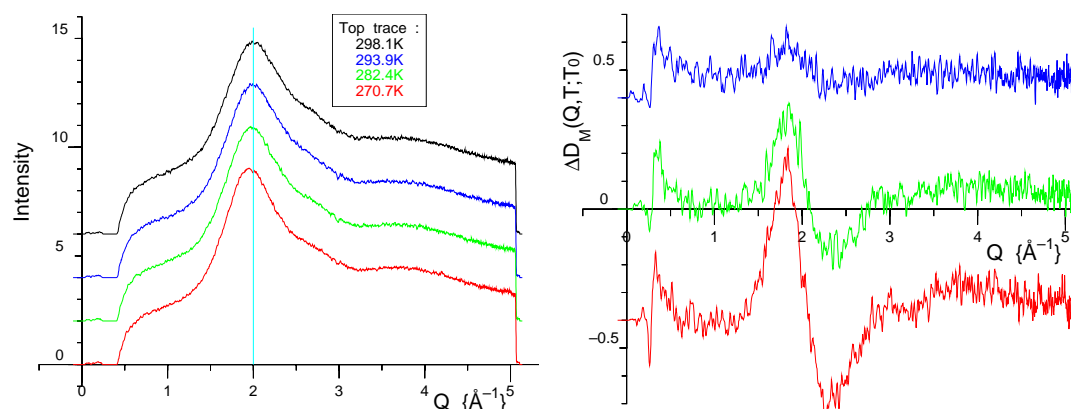
Figure 3. a) The diffraction pattern for the confined water at several temperatures (dry silica subtracted), b) the function, ΔD_M (Q ; ΔT), for the confined water with a reference temperature T_0=298K.
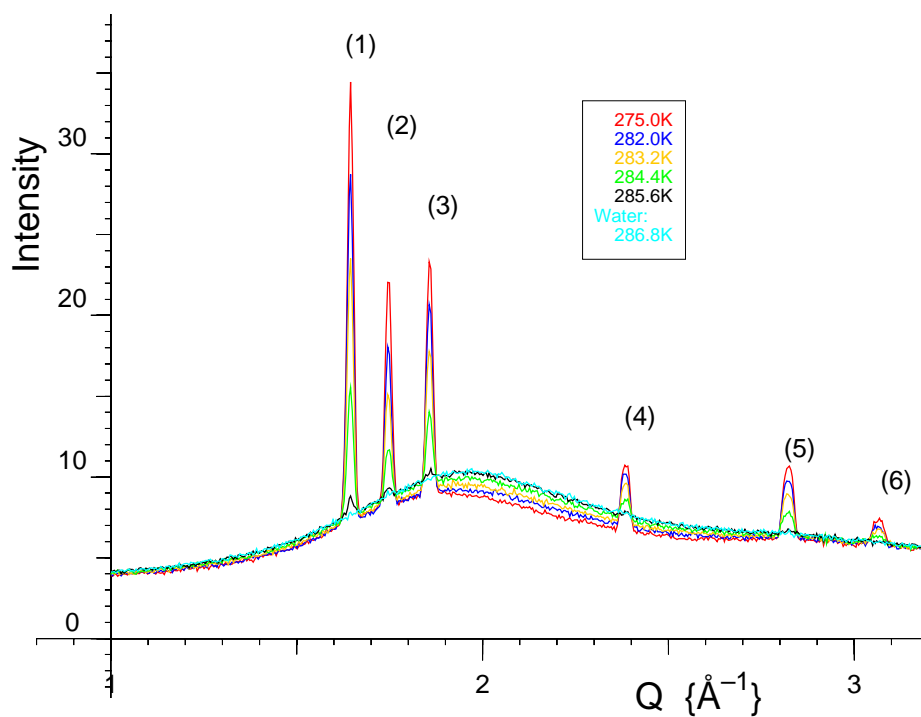
3.2. Hexagonal ice peaks

Temperature range B concerns the formation of hexagonal ice on the outside of the silica grains. Figure 4 shows a typical intensity pattern for temperature regime B and a Q-range incorporating peaks 1-6, where only the hexagonal crystalline form is present. Since there are no geometric constraints, the behaviour is close to that of the bulk water/ice phase and the characteristic triplet of (100), (002) and (101) peaks covering the range 1.65Å^{-1} to $1.86\text{Å}^{-1}$are observed in well-resolved manner. Three further peaks are also observed at Q-values of 2.39, 2.83 and 3.07 ($\pm$0.01) Å^{-1}, corresponding to (102), (110) and (103) indices, and it is convenient to consider these peaks first. Peaks 4 and 6 are signatures of hexagonal ice and do not occur for cubic ice but peak 5 arises for both hexagonal and cubic crystal structures.
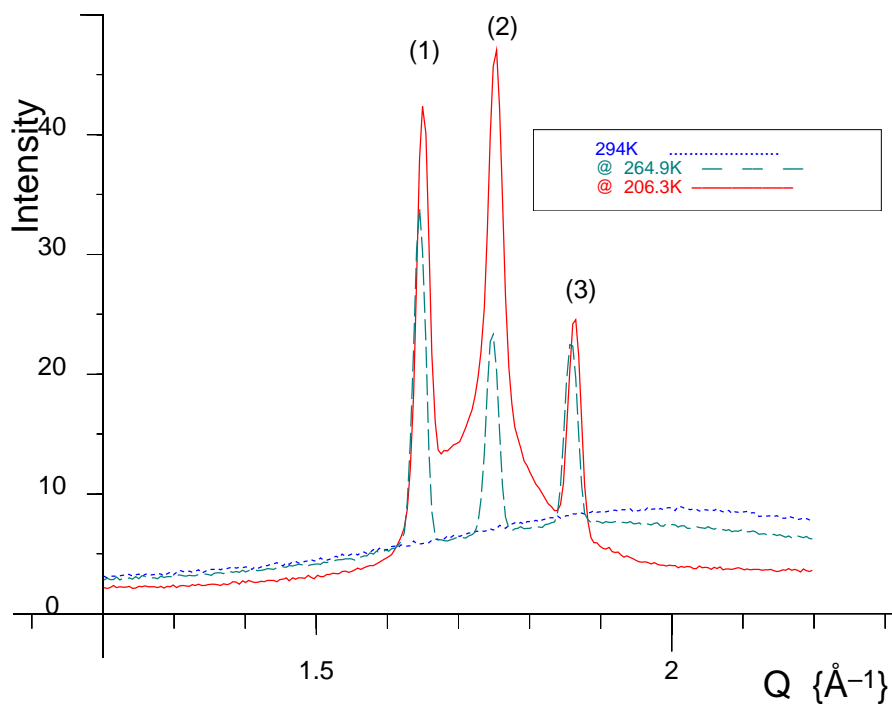
3.3. Cubic ice peaks

Ice I_c is formed in temperature range C. For pure cubic ice there should be a single peak in the centre of the triplet [position 2] and another peak at position 5. The data reveal the growth of a complex peak profile in the position of the triplet and the emergence of a very broad peak centred at $\sim$ 2.8 Å^{-1} in the region of peak 5. It therefore seems that the hexagonal ice peaks, formed initially, are much more intense than those of the cubic ice, which are also subject to diffraction broadening effects according to equation 5.

Figure 5 shows a typical intensity pattern for temperature regime A, B, C and a Q-range incorporating peaks 1-3. For temperature regime C, both crystalline forms are present.

Figure 4. The intensity profile of the hexagonal ice peaks [peaks 1-6] on a warming ramp.

Figure 5. A selected set of intensity profiles for the water, hexagonal and cubic ice peaks.

3.4. The triplet peak profile

The triplet peak is easy to analyse in range B as the individual peaks are well resolved but the complexity of the broad profile for the cubic ice formed in range C causes considerable problems. The approach adopted here has been to extrapolate the data from the hexagonal ice behaviour in range B into range C. In this way it is found that following the formation of the external ice, the intensity of the hexagonal ice peaks (parameter A of equation 7) further increases by about 15% as the temperature is reduced to $\sim$ 180K. The parameters σ and I_B were fixed at their values for region B. The peak position, Q_0 changes approximately linearly with temperature and its position can be accurately predicted.

The data have been fitted with 35 analytic quartic piecewise polynomials, continuous in amplitude and curvature, using 36 breakpoints suitably spaced over the range 1.0 to 3.3Å. This allowed the hexagonal ice pattern to be suitably scaled in Q to follow the displacement with temperature, and to be subtracted from the total pattern. The resulting pattern for the cubic ice, Figure 6, shows typical characteristics with a sharp peak at position 2 and a shoulder on the low-Q side. The broad peak 5 is clearly seen and peak 4, which is due to hexagonal ice alone, is eliminated.

As the temperature is reduced, the confined disordered water/ice is progressively converted to cubic ice. At lower temperatures the intensity of the cubic ice profile grows continuously, though more slowly. There is clear indication of the continuous formation of cubic ice without any change in the shape of the composite peak profile as the temperature is reduced. The differential function $\Delta D_M(Q, T; T_0)$ shown in figure 6 emphasises the gradual conversion of the broad water/disordered ice peak at $\sim 2\mathring{A}^{-1}$ to the crystalline form over an 80 K range.

Following the initial formation of the cubic ice at 258K it seems that the intensity increases by $\sim$45% over the range extending down to 150K. This unexpected behaviour is discussed in Section 4.3.

3.5. Lattice parameters

The change in the peak positions with temperature, $Q_0(\mathrm{T})$ gives a direct measurement of the variation in the lattice parameters and hence the expansion coefficients. The data are shown in Fig 7 as a plot of the fractional change in the position, $\frac{Q_0(T)}{Q_0(T_0)}$, against temperature where T_0 has arbitrarily been chosen to be 0°C. The data may be fitted by the quadratic relation

$$\frac{Q_0(T)}{Q_0(T_0)} = 1 + \alpha(T - T_0) + \beta(T - T_0)^2 \tag{5}$$

where α is the linear expansion coefficient and β the quadratic expansion coefficient. The extracted parameter values for each of the peaks are given in Table 2.

As expected the hexagonal ice on the outside of the pores behaves as if it were a bulk sample although the actual α-values are a little lower than those given in the literature (Rottger *et al.*, 1994). Since there is negligible diffraction broadening in the
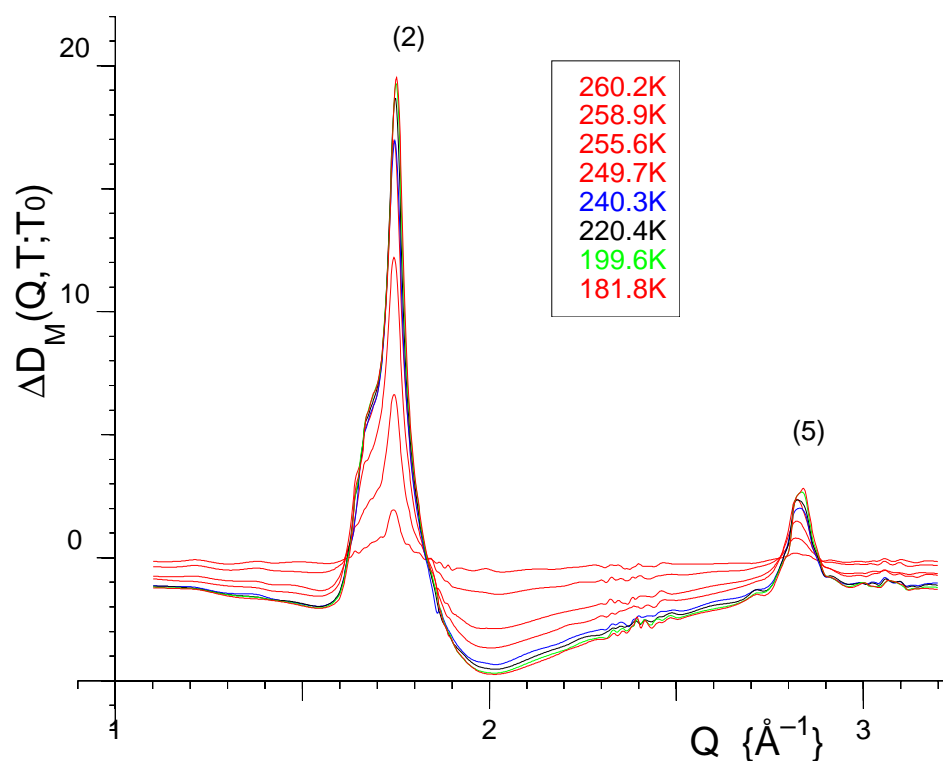
Figure 6. The changing profile of the cubic ice phase (see text for details).

diffraction peaks for this phase it must be assumed that the overall dimensions of these crystallites are relatively large compared to the intra-pore crystallites although they will be smaller than the normal crystals formed in a bulk phase nucleation process. The expansion coefficient for the cubic ice phase in the pores is difficult to extract from these measurements and will be considered in the treatment of the data for the partially-filled samples.

Peak No.	$Q_0(T_0)$ {Å^{-1}}	$10^6.\alpha$ {K^{-1}}	$10^8.\beta$ {K^{-2}}
1	1.645	-58.8	-18
2	1.746	-51.1	- 7
3	1.857	-53.6	-12
4	2.385	-55.0	-12.5
5	2.823	-55.3	-12
6	3.065	-52.6	- 8

Table 2. Peak positions Q_0 at $T_0 = 0°\text{C}$ and thermal expansion coefficients α and β for ice in the overfilled SBA-15 sample.
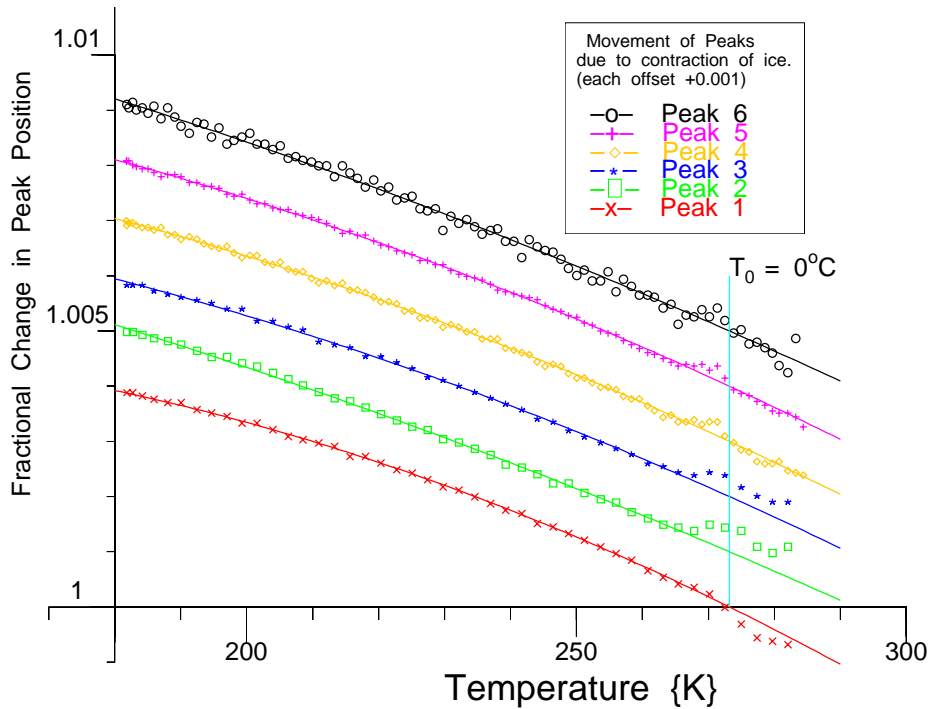
Figure 7. The relative variation of the various peak positions as a function of temperature; the fitted lines are for equation 8 with parameter given in table 2.

3.6. Dynamic features of the interfacial layer

The two overlapping sets of data for the variation of the T_2 relaxation rate with temperature are plotted together in Fig. 8. The NMR relaxation behaviour observed for the water/ice in the SBA-15 silica is dependent on temperature and as well as 'water-like' and 'ice-like' phases, a phase with intermediate properties is observed. Pure bulk water has a T_2 relaxation time of the order of a few seconds at the 0.5 T B_0 static magnetic field used for this relaxation work. However, in the pores of this SBA-15 silica, the surface relaxivity reduces the T_2 of the water to about 8ms. In comparison, the bulk phase of brittle ice has an approximately Gaussian free induction decay with a relaxation time of the order of 10μs.

The free induction decay for this sample at $\sim$190K is very similar to that of bulk ice, but as the temperature is raised by 20 K to 210K some of the brittle ice transforms to a component with a longer relaxation time and with a form that becomes increasingly exponential. Above 220 K, the shorter brittle ice component reduces in amplitude as it converts to the longer form, while the longer component of the FID remains fairly constant in relaxation time, between 100 to 200μs, and its amplitude progressively increases with temperature. Just below the melting temperature of the ice in the pores, at the Gibb-Thomson lowered temperature of about 260K, there is a rapid increase in the relaxation time of the longer component.

It is expected that the effects of confinement will alter the relaxation and a series of
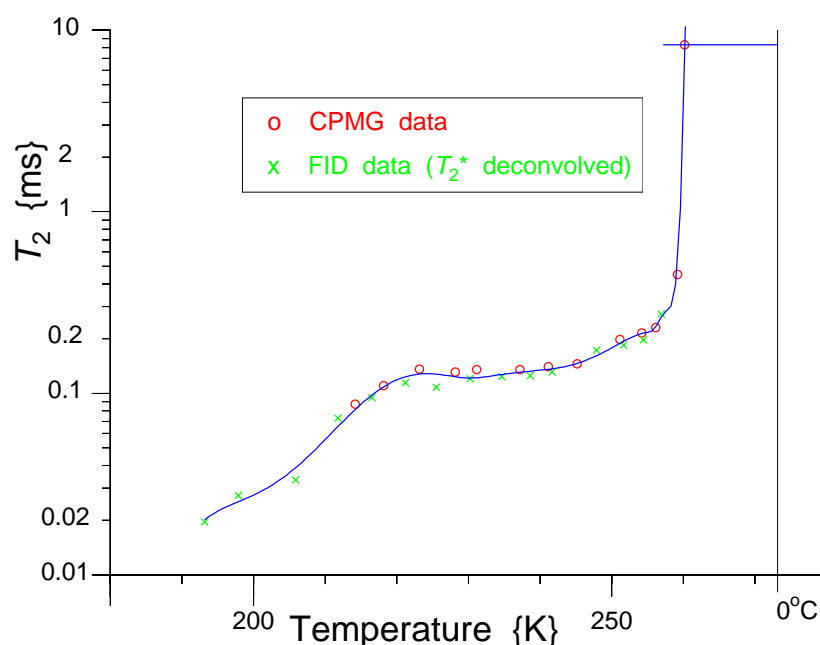
Figure 8.   The variation in the NMR proton T_2 relaxation time as a function of temperature for water/ice in SBA-15.

possible influences needs to be taken into account. However, the observed values seem to indicate a behaviour that can be broadly characterised as intermediate between a 'liquid-like' and 'solid-like' state. The T_2 values are different from those observed in region B for the cubic ice, implying that the dynamic features in the interfacial layer are intermediate between those applying to the normal behaviour of ice and water. These relaxation results for water and ice are also in agreement with spectroscopic studies of water in MCM-41 and SBA-15 (Grünberg *et al.*, 2004).

There are three possible causes that need to be considered for this factor of 10 increase in the T_2 at around 200K, for the defective ice, over that for brittle ice :

(i) T_2 relaxation is due to the dipolar interaction of one nuclear spin on another, an increase in the actual distance between the protons will lengthen T_2 . Given the observed changes as a function of temperature in figure 8 it is improbable that this behaviour is due to a simple lattice expansion.

(ii) There may be translational diffusion, giving rise to motional narrowing. This may be expected to play a part in the observed T_2, particularly given the large change in temperature and is the likely cause of the rapid change in T_2 in the vicinity of the melting point in the pores. However the observed behaviour of $T_2(T)$ over the range 180K to 250K is not characteristic of a translational activation energy, as would be expected for translational motional narrowing.

(iii) There may be rotational diffusion. In plastic crystals, rotation is well known to give rise to a form of motional averaging such that the actual proton separations must be replaced by the separation of the molecular centres. This gives rise to a

significant increase in T_2 at the onset of rotational motion, followed by a plateau in $T_2(T)$ as T increases (Chezeau and Strange, 1979).

The plot of $T_2(T)$ in figure 8 is very similar to that for the plastic phases of materials such as cyclohexane, showing the form of the above case (iii) with step and plateau, followed by the rapid rise of case (ii) just before melting; consequently it is suggested that this longer ice component is in a plastic crystalline state and corresponds to the disordered component as measured by neutron scattering.

The NMR measurements will be reported in detail in a separate paper; combined with the neutron data, they indicate that there is an equilibrium state within the interfacial layer in the pores, such that the ice changes continuously and reversibly with temperature between a brittle cubic crystalline phase (presumably mostly located in the centre of the pore) and a plastic disordered rotator phase (presumably mostly located near the silica surface of the pore).

It is clear that the dynamical behaviour of ice formed in a confined space is complex and further measurements will be needed to fully interpret all the current observations. The possibility of a plateau in the region of 200K is interesting as there are some unexplained features (Weik *et al.*, 2005) in the investigation of biological samples that have been 'fast frozen' and exhibit structural variation in this temperature region on heating. Related features have recently been reported for low filling-factors of water in Vicor (Zanotti *et al.*, 2005). The use of NMR as a complementary technique is clearly of great value in probing more closely into the characteristics of this intermediate 'water-ice' layer and further work is currently in progress.

4. Interpretation

4.1. Phase transformations and general features

The neutron diffraction results for the nucleation of ice in SBA silica follow the pattern previously observed for the MCM-41 and MCM-48 silicas (Dore *et al.*, 2002). In this study, the pore volume is over-filled and the initial changes refer to the freezing of water to hexagonal ice on the external surfaces of the silica grains. The behaviour is similar to that of bulk water although there is a more extensive super-cooling region for the cooling run, typically 15±5 K, which is probably due to the irregular external surface of the grains that does not allow the extended formation and growth of ice crystallites. However, the diffraction peaks do not show any diffraction broadening, so the crystallites are large compared with the dimensions of the pores. The liquid phase also shows normal behaviour with a monotonic change in the position of the main diffraction peak. Furthermore, the temperature difference function displays characteristics resembling those seen in many previous experiments.

The most interesting aspects of the new results concern the nucleation of ice within the pores. As previously observed for other mesoporous silicas, defective ice is created and the present datasets give an indication that the hexagonal ice on the external

surfaces cannot extend into the pore volume after the main nucleation event. However, DSC (Schreiber *et al.*, 2001), PVT measurements (Anderson *et al.*, 2003a,b) indicate that the external ice can play the role of initiator in the nucleation of the pore water and this process presumably occurs at the entrance of the pores. The intensities of the hexagonal ice peaks are unaltered as the temperature is further reduced so that there is a clear distinction between the 'external' and 'internal' forms of ice in the neutron measurements. Consequently, the growth process for the formation of ice in the pores is fundamentally different from that occurring in a bulk ice sample or for a thin layer on an open substrate.

'Cubic' ice may be formed from a number of different precursors and always seems to have a profile that incorporates an indication of residual hexagonal ice peaks with an asymmetric distribution. It has been suggested (Kuhs *et al.*, 1987) that this feature is due to the relatively large concentration of stacking faults that may contain some sequences with the hexagonal ice arrangement. However, a detailed analytic treatment of these crystallographic features has not been produced due to the complexity of the problem arising from the three-dimensional nature of this defect structure. The profile does seem to be dependent on the geometrical nature of the ice crystallites as shown by the nucleation of thin water films in partially-filled samples of sol-gel silicas with differing pore dimensions (Baker *et al.*, 1997; Morishige and Uematsu, 2005). Another consequence of the defective structure is the possibility of lattice defects such that proton transfer processes could be enhanced and lead to an anomalous value of the proton diffusion through the solid phase. This point is discussed further in Section 4.5.

4.2. Features of the cubic ice phase

The experimental data, shown in Fig 9, exhibit a gradual increase in the intensity of the cubic ice peaks as the temperature is reduced and a corresponding decrease when the temperature is raised. This behaviour is also seen in the studies of sol-gel and MCM silicas although the effect is much reduced. In the case of SBA-15, an additional complication arises from the fact that the pore volume is not made up of ideal cylindrical mesopores with a smooth surface. There is evidence (Joo *et al.*, 2002) that samples prepared by this route incorporate a pore volume with characteristics of a smaller pore dimension. The presence of this microporosity or roughness of the pore walls, as revealed by the nitrogen adsorption isotherm, indicates that ~ 24 % of the nitrogen molecules in the pores are in direct contact with the pore wall at complete pore filling (see Section 2.3). As mentioned in Section 2.3, the contribution to the total pore volume for the present SBA-15 sample is less than 5% from this effect. Furthermore, the failure to observe a second specific nucleation event below the formation of cubic ice in the primary pores also suggests that any effects due to this microporosity are negligible in the context of these observations. However, the shape of the curve in Figure 6 that relates directly to the amount of cubic ice in the available pore volume requires some form of explanation and is discussed in Section 4.4.
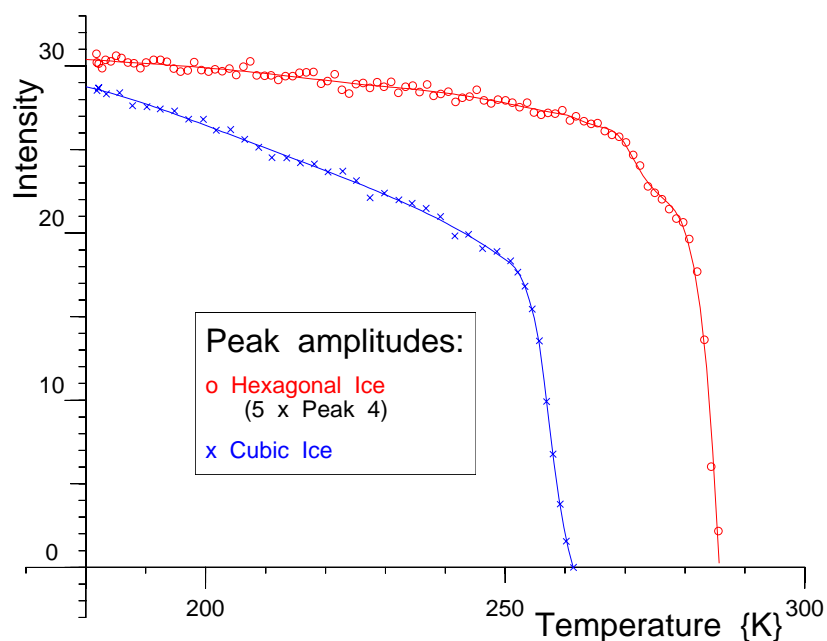
Figure 9. The change in the intensity of the cubic and hexagonal ice peaks as the temperature is increased.

4.3. Nucleation and growth of cubic ice

The formation of cubic ice in the pores rather than hexagonal ice has been attributed to restrictions on the size of the crystallite. The proto-crystallite that forms initially in the liquid phase is an assembly of hydrogen-bonded molecules with no particular orientation or defined lattice planes. As it increases in size, there is competition between the different growth axes resulting in a large concentration of stacking faults, i.e. there is no regular formation of hexagonal [abcabc] or cubic [ababab] lattice planes. Beyond a certain size, thought to be in the region of 300Å, growth in the hexagonal ice mode becomes dominant and a normal ice I_h crystal is formed. This process suggests that all ice crystals are initially formed from a defective ice crystallite but also that this component is not normally seen when the crystal becomes large. It is consequently only when the growth is restricted within the pore volume that the cubic ice component remains a significant proportion of the resulting volume of ice. This viewpoint is in good agreement with the computational studies of the nucleation process in water by Ohmine and co-workers (Matsumoto *et al.*, 2002) using molecular dynamics to observe the real-time changes that occur in the development of the hydrogen-bonded structures prior to crystallization.

It is interesting to note in this context that a pure form of cubic ice has never been observed experimentally. There are various routes leading to the formation of cubic ice but diffraction experiments that have appropriate Q-resolution always reveal an asymmetric peak profile with a shoulder on the low-Q side. Even in the case of the low temperature phase transformation of low-density amorphous ice (Blakey, 1994) it is seen

that the main peak has similar characteristics although there is no confining medium in this situation and the higher-order peaks are sharper, indicating larger crystallites. It is therefore reasonable to conclude that a defect-free form of cubic ice does not exist, naturally. However, the reasons for this behaviour remain unclear and it has not as yet been possible to investigate the defect structure by a modeling approach that attempts to fit the observed diffraction profile. It is possible that the quantitative data obtained in these experiments could provide a starting point for more detailed calculations.

4.4. Comparison with other studies

Two other diffraction studies of the water-to-ice transformation in mesoporous silicas, comparable to the present neutron study, have been reported (Morishige and Iwasaki, 2003; Morishige and Uematsu, 2005) using x-rays. The first work was based on the use of a variable filling factor, f, for an MCM-41 silica of 39Å pore size, where the diffraction pattern was broad and did not exhibit any evidence of Bragg peaks. The most recent one covers a range of silicas with pore diameters of 40-720Å and a fixed filling factor of 0.8, investigated at a number of static temperatures. The triplet profile shows the expected variation changing from a broad single peak [MCM-41; 44Å] through an asymmetric cubic ice shape [SBA-15; 98Å] to a hexagonal pattern [CPG] as the pore size is increased up to 720Å. The results for the 98Å sample of SBA-15 silica, taken at four different temperatures over the range 200-262K, show features similar to those seen in the present results. The authors discuss the reasons for the change in the profile due to the differing geometrical constraints, in terms of small crystallite size with a high concentration of stacking faults, as previously suggested. The authors distinguish between the predicted symmetric profile of central (111) peak that is not influenced by stacking faults and the asymmetric features of some other peaks. The resulting conclusion is that the crystallites could be more correctly described as defective hexagonal ice than cubic ice. However, it seems clear that there is agreement on the essential features relating to the high concentration of stacking faults and the fact that the reasons for this behaviour are still unknown. One point of difference in the interpretation of the nucleation process is apparent as it is suggested that the nucleation process occurs at the pore walls. Obviously, the position of the ice in the available pore volume is not determined by these experiments and it is difficult to think of a way in which this spatial information could be easily obtained.

The results of the neutron runs, using continuous temperature change, suggest a reversible process involving an equilibrium state for the quantity of ice. It therefore seems more appropriate to regard this transformation as a change in the properties of the ice/water interface with the silica, as discussed in the following section. Consequently, we believe that for filled or 'almost-filled' samples the initial ice formation may be seeded (Schreiber *et al.*, 2001) by the nucleated hexagonal ice outside the pores, which then grows as defective cubic ice along the centre of the cylindrical pore, possibly surrounded by a layer of disordered ice. Further information will be presented separately.

Both the neutron and x-ray data involve studies over a range of filling factors and reveal different characteristics for variable pore-filling that relate to the presence of either water droplets or a water film on the internal surface of the silica cylinders. It seems that the connectivity of the water volume has a direct effect on the nucleation process inside the pore volume. This observation is in accord with the earlier DSC studies reported by Findenegg and collaborators (Schreiber *et al.*, 2001) and with prior and current NMR studies (Webber and Dore, 2004). Furthermore, additional neutron measurements on the 86 Å silica used in the present measurements, that will be reported later, also reveal different behaviour from that of the 'over-filled' [i.e. f >1] case. It is found that the initial nucleation to produce cubic ice may be, surprisingly, followed by the continued growth of hexagonal ice down to 180K. Clearly the nucleation and growth processes in the SBA-15 silicas are quite complex when the pores are not completely filled and further work is needed to investigate the detailed characteristics. It seems likely that the distribution of the water within the pore volume can have a dramatic effect on the nucleation and growth properties; some further results for partially-filled SBA-15 samples will be presented in subsequent papers (Seyed-Yazdi *et al.*, in preparation).

4.5. Characteristics of the water-silica interface

The data in Figure 6 show a steady growth of cubic ice with reducing temperature below 250K. Accordingly, there must exist some 'reservoir' of 'disordered water/ice' that does not give sharp diffraction features in the higher temperature region but is available to become part of the cubic ice crystallite at lower temperatures. Such disordered water/ice decreases as the temperature is lowered but re-forms as the temperature is subsequently raised. The NMR relaxation data show that a highly mobile component exists over a similar temperature range. The most likely location of this reservoir is near the boundary layer of ice with the silica surface. This region has sometimes been called an 'unfreezable water layer' but the NMR data suggests that while considerably more mobile than brittle ice, this region (in the fully-filled pore) is more 'ice-like' than 'water-like'. This behaviour presumably arises from the hydrogen-bonding across any siloxyl groups at the surface with the water molecules in close proximity. The structure is disordered because the silica has an amorphous nature and there is no registry with the ordered arrangement of the ice lattice. Since the present measurements extend over a large temperature range below the main nucleation event it seems that the disordered region can be incorporated into the crystallite provided that the temperature is low enough. Consequently the changes that are observed in this temperature range appear to be highly sensitive to this interfacial region.

The results for the heating curve in this region show only a small temperature shift with respect to the cooling curve, which is consistent with the expected temperature lag in the sample. This observation indicates that hysteresis effects are minimal and therefore the changes do not arise from metastable or under-cooled states. It therefore seems that the interfacial region is a true equilibrium state with a thickness that varies

with temperature. Using the intensity values apparent from the figure, where the ice peak increases by $\sim$45% over the range 150-250K suggests that the interfacial region shrinks by $\sim$9 Å, corresponding to two or three monolayers of water molecules, as the 'disordered ice/water' is incorporated into the ice crystallite. This conclusion is in broad agreement with an interpretation based on the Gibbs Thomson effect (Webber and Dore, 2004).

The nature of this interfacial phase at much lower temperatures is open to question and it may be inappropriate to term it either 'water' or 'ice' in the conventional use of these words. However, it does seem to have a well-defined character and is created as an equilibrium state that is primarily dependent on temperature and not on sample history. We therefore provisionally introduce the term '*plastic ice*' in analogy with the plastic phase of other materials, such as cyclohexane, where there is substantial rotational motion within a defined crystal structure. Since the neutron diffraction data only reveal static or 'time-averaged' information, indicating that the substance is disordered, the specific characterisation of a plastic crystal phase requires additional experimental information. The distinction can only be considered in relation to the dynamical properties of this interfacial region. Some information on this interfacial phase and its dynamic behaviour is provided by the preliminary NMR measurements but further studies are in progress.

5. Conclusions and Future Experiments

The present study extends the general investigation of super-cooling and nucleation features for water in ordered mesoporous silicas. The present results for an over-filled sample confirm the general properties observed in earlier experiments on MCM-type silicas but extend the range to larger pore sizes. The specific conclusions are:-

- water inside the pores nucleates to produce a defective form of ice-I that is intermediate between hexagonal and cubic ice
- external water on the surface of the grains nucleates to the normal form of hexagonal ice and may subsequently initiate the nucleation of the pore water but does not grow into the pores
- after the main nucleation event, the amount of crystalline ice in the pores continues to grow as the temperature is further reduced
- there is an offset between the main pore melting and freezing events but the hysteresis effects for the disordered component are found to be small (<5K in this sample), indicating an equilibrium state for the interfacial region that varies with temperature.
- the observed features of the ice growth can be attributed to the incorporation of 'non-frozen water' or 'mobile ice' from the porous corona or highly corrugated surface of the pore wall into the ice phase in the pores.

- the interfacial layer between the ice crystallite and the silica walls exhibits features that are spatially disordered and more mobile than bulk ice and may tentatively be characterised as '*plastic ice*'

- the linear coefficient of expansion for the ice I$_h$ lattice on the surface of the silica grains is found to be a little lower than that for the bulk phase.

An novel analysis of this data in analogy with cryoporometric techniques, is presented concurrently (Webber and Dore, submitted). Additional experiments have also been conducted for partially-filled samples of water and ice in SBA silicas and will be reported separately (Seyed-Yazdi *et al.*, in preparation). One new feature that is emerging from the analysis of the further neutron measurements is a possible separation of nucleation and growth processes in the development of the ice volume during cooling under certain conditions. It also seems that a form of amorphous ice is present in some conditions, especially for cases involving lower filling-factors.

The behaviour of water at a hydrophilic interface has important implications for the role of confined water in a bio-sciences context. The ability to produce large surface areas for a controlled study of interfacial interactions should enable progress to be made for more complex systems. It is of considerable interest to be able to study the properties of water/ice at different interfaces and the SBA-15 silicas probably represent the most convenient system for extending the study through the 'functionalisation' of the interface. Unlike MCM silicas, the pore dimensions are sufficiently large for various molecules to be grafted onto the walls of the pores in order to modify the interactions with the adsorbed water without introducing a large change in the pore characteristics. There is a particular interest in the fabrication of completely hydrophobic surfaces for this purpose (Lefevre *et al.*, 2004) but careful environmental control will be needed to ensure that the water remains in the pores during experimental measurements. Clearly, there are many ways in which the current techniques of neutron diffraction and NMR relaxation measurements can be used to extend the present investigations to the behaviour of water/ice in a range of different mesoporous materials with variable surface interactions.

6. Acknowledgments

References

Anderson R, Llamedo M , Tohidi B and Burgass R W 2003a *Journal of Physical Chemistry B* **107** (15) 3500–3506

— 2003b *Journal of Physical Chemistry B* **107** (15) 3507–3514

Baker J M , Dore J C and Behrens P 1997 *J. Phys. Chem. B* **101** (32) 6226–6229

Beck J S, Vartuli J C and Roth et al W J 1992 *Journal Of The American Chemical Society* **114** (27) 10834–10843

Blakey D M 1994 *Structural studies of vapour-deposited amorphous-ice and argon/amorphous-ice systems by neutron diffraction.* Phd Physics University of Kent at Canterbury, UK.

Booth H F and Strange J H 1998 *Magn. Reson. Imaging.* **16** (5-6) 501–504

Brownstein K R and Tarr C E 1977 *J. Magn. Resn.* **26** 17–24

Chezeau J M and Strange J H 1979 *Physics Reports - Review Section of Physics Letters* **53** (1) 1–92

Dore J 2000 *Chem. Phys.* **258** (2-3) 327–347

Dore J C, Haggenmller C, Behrens P and Fisher H 1999 *ILL Annual Report* 28URL `http://www.ill.fr/AR-99/page/34liquids.htm`

Dore John, Webber Beau, Hartl Monika, Behrens Peter and Hansen Thomas 2002 *Physica A* **314** (1-4) 501–507

Dore J C, Webber J B W and Strange J H 2004 *Colloids and Surfaces A: Physicochem. and Eng. Aspects* **241** (1-3) 191–200. URL `http://dx.doi.org/10.1016/j.colsurfa.2004.04.005`

Grünberg B, Emmler T, Gedat E , Shenderovich I, Findenegg G H , Limbach H -H and Buntkowsky G 2004 *Chemistry-A European Journal* **10** (22) 5689–5696

Hansen T 2004 URL `http://whisky.ill.fr/YellowBook/D20/`. The D20 instrument description.

Impéror-Clerc M , Davidson P and Davidson A 2000 *Journal Of The American Chemical Society* **122** (48) 11925–11933

Joo S H , Ryoo R, Kruk M and Jaroniec M 2002 *J PHYS CHEM B* **106** (18) 4640–4646

Kruk M, Jaroniec M and Sayari A 1997 *Langmuir* **13** (23) 6267–6273

Kuhs W F, Bliss D V and Finney J L 1987 *Journal De Physique* **48** (c-1) 631–636

Lefevre B , Saugey A, Barrat J L and et al 2004 *Colloids and Surfaces A-Physicochemical and Engineering Aspects* **241** (1-3) 265–272

Liu Eric 2003 *Synthesis of ordered mesoporous aluminium oxide using novel templating techniques, and the characterisation of nucleation of ice in mesoporous silica.* Msc Physics University of Kent at Canterbury, UK.

Matsumoto M , Saito S and Ohmine I 2002 *Nature* **416** (6879) 409–413

Morineau D and Alba-Simionesco C 2003 *J. Chem. Phys.* **118** (20) 9389–9400

Morishige K and Iwasaki H 2003 *Langmuir* **19** (7) 2808–2811

Morishige K and Uematsu H 2005 *Journal Of Chemical Physics* **122** (4) Art. No. 044711

Rottger K , Endriss A and Ihringer et al J 1994 *Acta Crystallographica* **Section B-structural Science** (50) 644–648

Schreiber A , Ketelsen I and Findenegg G H 2001 *Physical Chemistry Chemical Physics* **3** (7) 1185–1195

Schreiber A , Ketelsen I, Findenegg G H and Hoinkis E 2006 Llewellyn P L , Rouguerol J , Rodrigues-Reinosi F and Seaton N A, eds., *Characterization of Porous Solids* vol. VII. 17–24

Seyed-Yazdi J , Dore J C, Webber J B W and Findenegg G in preparation

Shenderovich I, Buntkowsky G, Schreiber A , Gedat E , Sharif S, Albrecht J, Golubev N S , Findenegg G H and Limbach H -H 2003 *Journal Of Physical Chemistry B* **107** (43) 11924–11939

Strange J H , Mitchell J and Webber J B W 2003 *Magn. Reson. Imaging* **21** (3-4) 221–226

Strange J H , Rahman M and Smith E G 1993 *Phys. Rev. Let.* **71** (21) 3589–3591

Webber Beau and Dore John 2004 *Journal of Physics: Condensed Matter* **16** (Special Issue: Water in Confined Geometry) S5449–S5470. URL `http://stacks.iop.org/JPhysCM/16/S5449`

Webber J B W 2000 *The Characterisation of Porous Media*. Phd Physics University of Kent at Canterbury, UK. . URL `http://www.kent.ac.uk/physical-sciences/publications/theses/jbww.html`

— 2003 *Magn. Reson. Imaging* **21** (3-4) 428. URL `http://dx.doi.org/10.1016/S0730-725X(03)00172-3`

Webber J B W and Dore J C submitted

Webber J B W, Strange J H and Dore J C 2001 *Mag. Res. Imag.* **19** (3-4) 395–399

Weik M, Lehnert U and Zaccai G 2005 *Biophysical Journal* **89** 3639–3646

Wright John D and Sommerdijk Nico A J M 2000 *Sol-Gel Materials: Chemistry and Applications*. New dover edn. CRC Pr I Llc. ISBN 9056993267

Zanotti J M , Bellissent-Funel M C and Chen S H 2005 *Europhysics Letters* **71** (1) 91–97

Zhao D Y, Feng J L and Huo Q S et al 1998a *Science* **279** (5350) 548–552

Zhao D Y, Huo Q S and Feng J L et al 1998b *Journal Of The American Chemical Society* **120** (24) 6024–6036

Zickler G A , Jähnert S , Wagermaier W, Funari S S, Findenegg G H and Paris O 2006 *Phys. Rev. B.* **73** 184109